Journal of Nuclear Materials 390–391 (2009) 223–226

Contents lists available at ScienceDirect

Journal of Nuclear Materials

journal homepage: www.elsevier.com/locate/jnucmat

Impurity production and acceleration in CTIX

D. Buchenauer [a,*], W.M. Clift [a], R. Klauser [b], R.D. Horton [b], S.J. Howard [c], S.J. Brockington [d], R.W. Evans [b], D.Q. Hwang [b]

[a] Sandia National Laboratories, MS-9161, P.O. Box 969, Livermore, CA 94550, USA
[b] CTIX Group, University of California at Davis, Davis, CA 95616, USA
[c] General Fusion Inc., Burnaby, Canada BC V5A 3H4
[d] HyperV Technologies Corp., Chantilly, VA 20151, USA

ARTICLE INFO

PACS:
52.55.Hc
52.70.−m
52.25.Vy

ABSTRACT

The Compact Toroid Injection Experiment (CTIX) produces a high density, high velocity hydrogen plasma that maintains its configuration in free space on a MHD resistive time scale. In order to study the production and acceleration of impurities in the injector, several sets of silicon collector probes were exposed to spheromak-like CT's exiting the accelerator. Elemental analysis by Auger Electron Spectroscopy indicated the presence of O, Al, Fe, and Cu in films up to 200 Å thickness (1000 CT interactions). Using a smaller number of CT interactions (10–20), implantation of Fe and Cu was measured by Auger depth profiling. The amount of impurities was found to increase with accelerating voltage and number of CT interactions while use of a solenoidal field reduced the amount. Comparison of the implanted Fe and Cu with TRIM simulations indicated that the impurities were traveling more slowly than the hydrogen CT.

1. Introduction

The main requirement for fueling by a compact toroid (CT) plasma is that the velocity of the CT be large enough (~50 cm/μs) to balance the kinetic energy ($\frac{1}{2}\rho_{CT}V_{CT}^2$) against the tokamak's magnetic field energy ($B^2/2\mu_0$). Given the difficulty to achieve central fueling for large tokamaks such as ITER, several experiments have pursued spheromak-like CT injection. The initial demonstration of density increase on TdeV [1] has been followed by experiments on JFT-2M [2] and STOR-M [3], and design work for the LHD stellarator [4]. Steering by use of magnetic switching [5] and fundamental CT formation and acceleration studies are also in progress [6]. Magnetic probes and optical techniques have been the primary diagnostics.

Since electrodes are used in the CT accelerator, the potential for impurity generation through plasma–surface interactions requires study. Early work on the CTIX accelerator showed that oxygen may be trailing the main plasma (not fully accelerated to V_{CT}) [7]. This is important since if impurities are contained within the main CT, their high velocity and entrapment by the CT's internal magnetic fields would contribute to core tokamak impurity levels. These fields would not be present in the trailing plasma.

The present study uses a set of silicon collector probes to measure the relative amount of various elemental species deposited by the CT. Unlike similar measurements done on fusion experiments [8,9], the CT plasma energy density is sufficiently low that direct interaction of the CT with the collector can be used. Measurements of the collected species were performed using Auger Electron Spectroscopy (AES) sputter profiles and the depth of implanted species was modeled using TRIM.

2. Experimental setup

CTIX [7] uses two capacitor banks (a formation bank, here with $V_{form} = 7$ kV, and an acceleration bank, here with V_{acc} either 9 or 12 kV), a bias field, and a passive switching technique to form and accelerate moderate size ($r_i = 6.3$ cm; $r_o = 15.2$ cm) hydrogen plasmas. The CT axial velocity (V_{CT}) is determined from the arrival time on magnetic probes (B_z is measured 57, 91, and 142 cm from the gun end). Typical parameters for the CT are $V_{CT} \approx 20$ cm/μs, $L_{CT} \approx 30$ cm, $n_e \approx 10^{14}$ cm^3, and $T_e \approx 30$ eV. Although the ion temperature is not measured, the high velocity of the CT results in substantial translational kinetic energy for the ions (≈200 eV for H). After acceleration (center electrode end at $z = 169$ cm), the CT plasmas drift in a guide tube until reaching an experimental chamber (at $z = 212$ cm), where various diagnostics can be used. For the relatively low density CT's used in this study, the response of the interferometer was not adequate for characterization.

As the CT resistively decays following acceleration, the plasma expands in the guide tube (inward in radius) and experimental chamber (outward in radius). Two axially-separated ports on the

* Corresponding author.
E-mail address: dabuche@sandia.gov (D. Buchenauer).

0022-3115/$ - see front matter © 2009 Elsevier B.V. All rights reserved.
doi:10.1016/j.jnucmat.2009.01.058

experimental chamber allowed for insertion of a manipulator and interception of the plasma by a set of silicon collector probes (5.9 cm or 44.7 cm from the end of the guide tube). The two positions were used to verify that the magnetic field did not appreciably slow the ion impact into the silicon, since the field is very small at the far position. For each exposure, a radial set of five Si⟨1 1 1⟩ samples (.6 cm diameter and .15 cm thick) was vertically mounted vertically (2 cm spatial resolution). The innermost sample was located at $r = 2$ cm and the samples were numbered 1 through 5 (radially outward).

The samples were prepared by ultrasonically cleaning with alcohol before mounting. Auger depth profiling of prepared but unexposed samples indicated about 13 Å of SiO_2, with a small amount of carbon in the near surface. For Auger depth profiling to be useful, it is necessary that the sample does not heat or sputter during the exposure. Using a 1-d thermal model, the surface temperature rise was found to be as large as 180 K, however, it rapidly decayed following the 1.5 μs plasma exposure. The effect of hydrogen sputtering was modeled using the CT parameters and the TRIM code and found to be <.06 Å/shot. Sputtering from impurities would be much smaller due to their lower concentration in the plasma.

While CTIX does not presently inject CT's into a tokamak magnetic field, the influence of a magnetic field on the impurity transport was investigated by use of a coaxial solenoid coil (330 G on axis, $L_c = 30$ cm, located at $z = 186$ cm). This field is much lower than the internal fields of the CT and can easily be excluded as the main CT passes by. Impurities contained in any trailing plasma would be affected due to the much lower fields behind the CT.

3. Experimental results

The first exposures were used to determine what species were present and how the amount varied with the number of CT interactions. An Auger depth profile from exposure #1 (sample #1), consisting of 1000 CT plasmas is shown in Fig. 1. Here the relative atomic concentrations of O, Al, Fe, and Cu are plotted as a function of depth (depth scale calibrated by profilometry of a separate sputter crater). It should be noted that the Al Auger line is shifted in energy consistent with the shift being due to oxidation. Also shown in the inset is the radial variation of the film thickness, giving a scale-length comparable to the CT radius. It is interesting to evaluate what impurity level this might imply for the average CT, with aluminum oxide as the main impurity. Using full density Al_2O_3, a 200 Å thick film would result from 1000 shots of 9×10^{13} Al atoms cm^{-2}. If this amount was distributed uniformly throughout a CT, it would imply an Al impurity level of a few percent. Evidence below, however, indicates that the impurities are not traveling with the full CT velocity.

Table 1 lists the CTIX parameters used for all eight exposures (all performed with $V_{form} = 7$ kV). The first four exposures were used to vary the number of shots and check reproducibility. Using 10–20 exposures allowed for measurable Auger profiles of the impurities while, in most cases, not indicating an impurity film buildup on the surface (a film was found for exposures #1 and #5). Fig. 2 shows an Auger depth profile from exposure #2, sample #1 (10 shots), where implantation into the silicon sample of high mass species was observed. For fluxes low enough to prevent the impurity surface film, implantation depths on the order of 10–200 Å are expected from TRIM calculations (see below), and higher masses are expected to implant more deeply (for $V_i = V_{CT}$).

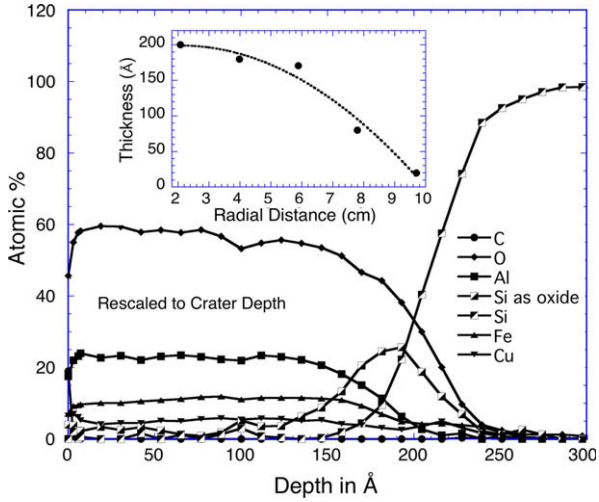

Fig. 1. Auger depth profile for exposure #1, sample #1, showing a 200 Å thick film of O, Al, Fe, and Cu. The inset shows the radial profile of the film thickness.

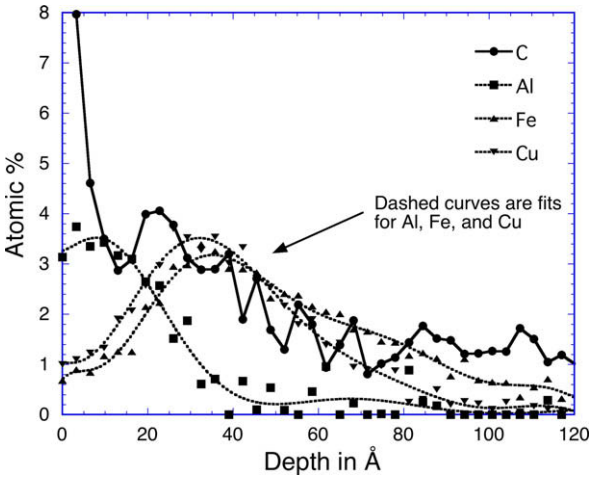

Fig. 2. Auger depth profile of exposure #2, sample #1, showing C and Al at the surface and Fe and Cu implanted into the sample. Si and SiO_2 add to a constant 90% to about 40 Å into the surface.

Table 1
Amount of impurities for each exposure, based on implantation width and concentration in silicon. Film refers to a buildup of impurities on the surface of the silicon.

Exposure	Number of shots	V_{acc} (kV)	Coil	Position (cm)	⟨V_{CT}⟩ (cm/μs)	Amount (arb. units)			Comment
						Al	Fe	Cu	
1	1000	9		5.9	–	–	–	–	200 Å film
2	10	9		5.9	17.9 ± 3.6	96	181	202	Only three samples
3	10	9		5.9	16.9 ± 4.2	62	164	136	
4	20	9		5.9	15.9 ± 3.3	148	352	247	
5	20	12		5.9	21.9 ± 5.6	–	–	–	Surface film
6	20	12	On	5.9	20.2 ± 5.7	157	626	291	
7	20	12		44.7	21.2 ± 5.1	92	242	146	
8	20	12	On	44.7	19.2 ± 4.5	45	155	93	

Table 2
Depth of impurity implants and inferred impurity velocities. Film refers to a buildup of impurities on the surface of the silicon.

Exposure	V_{acc} (kV)	Coil	Position (cm)	$\langle V_{CT}\rangle$ (cm/μs)	$d_{Auger,Fe}$ (Å)	$d_{Auger,Cu}$ (Å)	$\langle V_{inf,Fe}\rangle$ (cm/μs)	$\langle V_{inf,Cu}\rangle$ (cm/μs)	Comment
3	9		5.9	16.9 ± 4.2	32 ± 4	28 ± 6	6.6	5.1	
4	9		5.9	15.9 ± 3.3	39 ± 3	34 ± 4	8.6	6.8	
5	12		5.9	21.9 ± 5.6	–	–	–	–	Film
6	12	On	5.9	20.2 ± 5.7	40 ± 3	30 ± 2	9.8	6.7	
7	12		44.7	21.2 ± 5.1	41 ± 5	36 ± 7	9.1	7.3	
8	12	On	44.7	19.2 ± 4.5	34 ± 2	33 ± 4	7.8	6.6	

Since the concentrations of implanted impurities are small compared with the Si and SiO_2 levels, an estimate of the amount of impurities was determined from the peak concentration and width, averaged over samples 1–4 (amount = peak × width at half maximum). The amounts are listed in Table 1 for Al, Fe, and Cu. Although the amounts are not listed for exposure #5, these samples showed the highest amount of impurities, except for exposure #1. Also note that the amounts listed for exposure #2 are somewhat higher as they are averaged over only the first three samples. The amounts for oxygen and carbon were not listed; oxygen is present as a background gas and may become incorporated between shots or following exposure. Carbon was also present on the surface prior to exposure. It should also be noted that the depth scale in Fig. 2 was normalized for SiO_2 sputtering, so that it is valid to within 10% (the difference between Si and SiO_2 removal rates in the Auger system).

Most of the exposures consisted of 20 shots to optimize the statistical variation observed in both CT velocities and amounts of impurities found. By comparing pairs of exposures in Table 1, one can observe that the amount of impurities increases with number of shots (exposures 3 and 4) and increases with higher accelerating voltage (exposures 4 and 5; the film has a much higher amount of impurities than the samples showing only a few percent of implanted impurity species). The table also shows that the amount decreases as the probe position is moved further from the CT gun (exposures 6 and 8) and decreases when the coaxial coil is used (exposures 7 and 8).

4. Implantation results and modeling

The tendency for Fe and Cu to implant more deeply was observed on all samples and exposures except for exposure #1. The results are summarized in Table 2, where experimental conditions are listed for exposures 3–8, along with the average CT velocities $\langle V_{CT}\rangle$ and the Fe and Cu peak depths ($d_{Auger,Fe}$ and $d_{Auger,Cu}$). Here the depth refers to the average peak depth observed for samples 1–4 on each exposure, as there was no systematic variation of this depth with radius. While there is scatter in the data, some interesting results can be obtained. The shallowest peak depths for both Fe and Cu occur for the 9 kV accelerating voltage while the deepest values are found at 12 kV. Comparison of exposures 6 and 8 indicate that the depth of Fe and Cu is not significantly reduced as the CT travels in the experimental chamber. This rules out the possibility that the impurities are entrained within the CT and the magnetic field interaction with the sample reduces their impact velocity (compared to $\langle V_{CT}\rangle$). Also, comparison of exposures 7 and 8 indicate that use of the coaxial solenoid coil, which decreased the amount of impurities, did not strongly affect the depth of the Fe and Cu.

Fig. 3 shows the implantation that might be expected for exposure #4, as simulated by using TRIM (TRVMC98). Here a distribution of impurity velocities corresponding to the experimentally measured CT velocities was used, with constant amount of impurity per shot. This assumption is justified by the scaling of Fe and Cu amounts found in Table 1 for exposures 3 and 4 (factor of 2 increase). As expected, higher masses implant more deeply, however, the simulated peak depth for Fe and Cu is significantly larger than the Auger measurement. TRIM simulations showed that this difference occurred for all samples where implantation of Fe and Cu was observed.

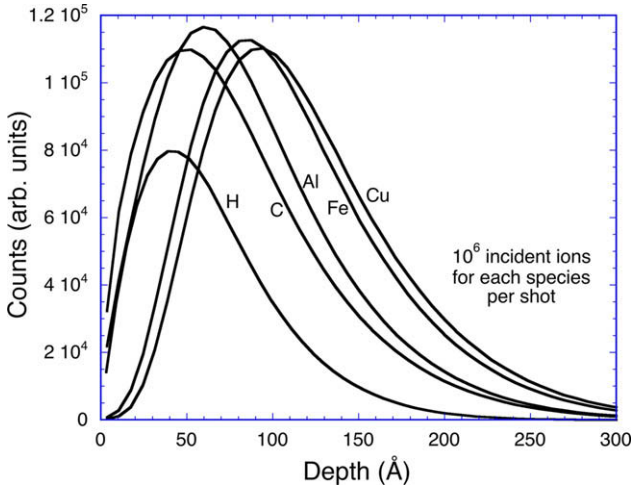

Fig. 3. TRIM simulation of implanted species traveling with the full CT velocity (exposure #4).

To estimate the velocity of the observed Fe and Cu implants, the distribution of CT velocities used for the TRIM simulations was lowered, keeping the same shape, but resulting in a reduced average impurity velocity ($\langle V_{red}\rangle$). This was done to simulate the lower velocities expected in the trailing plasma. Due to the lower velocities, the effect of the SiO_2 layer was included, although the effect was small. Fig. 4 shows the resulting peak depth dependence on reduced impurity velocity for exposure #4. Also shown is the range

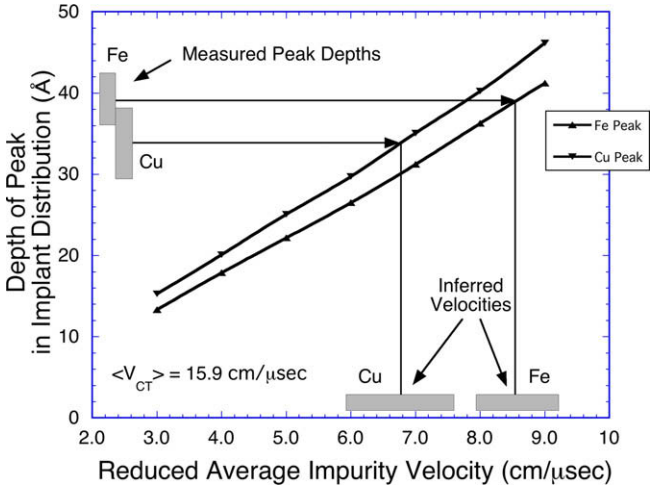

Fig. 4. Peak depth of Cu and Fe implants simulated by TRIM with reduced impurity velocities (exposure #4). Also shown are the inferred impurity velocities corresponding to peak depths observed in the Auger depth profiles.

of experimental peak depths for this exposure. The observed depths would correspond to inferred impurity velocities ($\langle V_{inf,Fe}\rangle$ and $\langle V_{inf,Cu}\rangle$) about half the average CT velocity (8.6 cm/μs for Fe; 6.8 cm/μs for Cu). Table 2 further lists the reduced impurity velocities that are inferred for exposure 3–8. Care should be used for exposure #3 as only 10 shots were used for the exposure and the effect of a single low velocity CT can skew the results. In all cases, the inferred impurity velocities for Fe and Cu are significantly lower than the average CT velocity. It should also be noted that the inferred width of the implant distribution is narrower than the corresponding Auger depth profile width. Since the impurities are trailing the CT, they are more likely to have a broader distribution of velocities than the CT.

5. Discussion and summary

The CTIX plasma facing surfaces consist mainly of 304 stainless steel, with small regions where copper is used in vacuum breaks. There are also regions of the inner electrode which have a coloration indicative of underlying copper being exposed. It cannot be determined from these measurements where the copper originates, but iron is likely coming from the electrode surfaces. The inferred velocities for the Fe and Cu indicates that these impurities are not contained within the CT, but experience a reduced accelerating force due to the smaller currents supported by the trailing plasma. It is interesting that the Auger peak depth for iron is always deeper than for copper, although if they had the same velocity, one would expect the reverse. This may indicate that the copper enters the trailing plasma later than the iron.

The aluminum observed almost certainly originates from alumina shields used to protect magnetic probes. The oxide shift of the aluminum in the Auger measurement may be due to direct alumina sputtering/evaporation, or it may oxidize between shots. Since aluminum is expected to be implanted at very shallow depths, the Auger depth profiles are not helpful in resolving how aluminum is being eroded (Al was found on the surface of all exposed samples). Since magnetic probes can be retracted, it should be possible in future experiments to strongly reduce the aluminum influx.

Several exposures also showed carbon at the surface, with hints of a subsurface peak positioned between the surface and the Cu and Fe peaks. Further experiments aimed at introducing carbon directly into CTIX plasmas are in progress.

In summary, we have performed the first direct measurements of impurities generated by a spheromak-like CT accelerator using collector probes. The intrinsic impurities originate from electrode and other plasma facing materials and scale with increasing number of shots and acceleration voltage. Under several conditions, implantation of high mass elements (Fe and Cu) gives an indication of high velocities, however comparison with TRIM simulations shows that they do not travel with the full CT velocity. Use of a modest axial magnetic field (≈10% of the CT's internal field) is effective in reducing the amount of the impurities by a factor 1.5–2.0. This field is expected to have a much stronger effect on the unmagnetized trailing plasma.

Acknowledgement

This work was supported by the US Department of Energy under contracts DE-AC04-94AL85000 and FG02-03ER54732.

References

[1] R. Raman, F. Marton, E. Haddad, M. St-Onge, G. Abel, C. Cote, N. Richard, N. Blanchard, H.H. Mai, B. Quirion, J.-L. LaChambre, J.-L. Gauvreau, G.W. Pacher, R. Decoste, P.J. Gierszewski, D.Q. Hwang, A. Hirose, S. Savoie, B.-J. LeBlanc, H. McLean, C. Xiao, B.L. Stansfield, A. Cote, D. Michaud, M. Chartre, Nucl. Fus. 37 (1997) 967.
[2] N. Fukumoto, H. Ogawa, M. Nagata, T. Uyama, T. Shibata, Y. Kashiwa, S. Suzuki, Y. Kusama, Fus. Eng. Design 81 (2006) 2849.
[3] D. Liu, C. Xiao, A.K. Singh, A. Hirose, Nucl. Fus. 46 (2006) 104.
[4] J. Miyazawa, H. Yamada, K. Yasui, S. Kato, N. Fukumoto, M. Nagata, T. Uyama, Fus. Eng. Design 54 (2001) 1.
[5] N. Fukumoto, Y. Inoo, M. Nomura, M. Nagata, T. Uyama, H. Ogawa, H. Kimura, U. Uehara, T. Shibata, Y. Kashiwa, S. Suzuki, S. Kasai, JFT-2M Group, Nucl. Fusion 44 (2004) 982.
[6] D.Q. Hwang, R.D. Horton, R.W. Evans, S. Howard, S. Brockington, J. Fus. Energy 27 (2008) 53.
[7] H.S. McLean, D.Q. Hwang, R.D. Horton, R.W. Evans, S.D. Terry, Fusion Technol. 33 (1998) 252.
[8] R. Bastasz, T.E. Clayton, J. Nucl. Mater. 145–147 (1987) 476.
[9] S.J. Kilpatrick, H.F. Dylla, W.R. Wampler, D.M. Manos, S.A. Cohen, R. Bastasz, J. Nucl. Mater. 162–164 (1989) 757.